ARTHEMIS

Assessment of Radiation damage and Transmutation Helium Effects on structural reactor materials via MIcromechanical testing and advanced analysis methodS

This project has received funding from the European Union's NextGenerationEU through the Recovery and Resilience Plan for Slovakia under project No. 09I03-03-V04-00384.

Deliverable D1.2

Microstructural Characterization and Nanoindentation of Ion-Irradiated Specimens

---

Lead author: Zoltán Száraz

ATRI
Advanced Technologies Research Institute

Table of contents

1. Introduction 3
2. Materials 4
3. Microstructural analysis 5
4. Nanoindentation testing 10
4.1. Experiments 10
4.2. Results 12
5. Summary 16
6. References 17

1. Introduction

The reliable operation of advanced nuclear systems depends on the availability of structural materials that can withstand extreme environments involving high radiation fields, transmutation effects, and corrosive coolants. A major concern is the accumulation of radiation-induced defects and helium, which can significantly alter mechanical properties, leading to hardening, embrittlement, and reduced service lifetimes. Understanding these degradation mechanisms at both the microstructural and mechanical levels is therefore essential for guiding the selection and qualification of materials for fission and fusion applications.

Ion irradiation offers an accelerated pathway to simulate neutron-induced damage and helium production in controlled laboratory conditions. Within the ARTHEMIS project, multi-step, multi-ion irradiation strategies have been developed to produce quasi-homogeneous damaged layers with controlled helium-to-displacement-per-atom (He/DPA) ratios. These irradiated specimens provide a well-defined platform to study the correlation between microstructural changes and macroscopic mechanical behavior.

This report presents the results of comprehensive post-irradiation evaluations carried out on both as-received and ion-irradiated specimens. The microstructural characterization employed a suite of complementary techniques—including Scanning Electron Microscopy (SEM), Transmission Electron Microscopy (TEM), Positron Annihilation Spectroscopy (PAS), and Small-Angle Neutron Scattering (SANS)—to reveal defect structures, phase stability, and helium bubble formation. In parallel, nanoindentation experiments, including trapezoidal and depth-resolved quasi-static tests, were conducted to quantify irradiation-induced hardening and to provide localized stress–strain response data.

By combining advanced microstructural analysis with micromechanical testing, this work provides critical insights into the mechanisms of irradiation-induced property changes. The findings contribute directly to the ARTHEMIS objectives of establishing robust methodologies for evaluating irradiation damage, helium effects, and their implications for the performance of candidate materials in future nuclear systems.

2. Materials

This study focuses on two key structural materials of high relevance for advanced nuclear systems:

- Alloy 800H – a high-chromium, high-nickel austenitic steel (~20 wt.% Cr, ~32 wt.% Ni) that plays a central role in innovative supercritical water-cooled small modular reactor (SCW-SMR) designs and is also of interest for the GEN IV Very High Temperature Reactor (VHTR) concept.
- EUROFER97 – a reduced activation ferritic-martensitic (RAFM) steel containing ~9 wt.% Cr and no Ni, widely studied as a candidate material for both fission and fusion applications.

The chemical compositions of both materials are summarized in Table 1.

The EUROFER97 material was available in sheet form and sectioned into specimens of 8 × 8 × 0.5 mm^3. The 800H alloy, provided via the ECC-SMART Euratom project, was supplied as rods and processed into two specimen geometries: disks of 10 mm diameter and 1 mm thickness, and corrosion coupons measuring 10 × 15 × 2 mm^3.

Prior to ion-irradiation, all samples underwent surface preparation. Mechanical polishing was first carried out using SiC sandpapers of progressively finer grit (600–4000), followed by final polishing to a mirror finish using 1 µm diamond suspension. This ensured surface quality is suitable for both ion implantation and subsequent microstructural and micromechanical characterization.

Table 1. Chemical composition in wt%.

Steel	Cr	Ni	Al	W	Si	Mn	C	Ti	V	Ta	Fe
Eurofer97	**8.9**	**-**	**-**	**1.1**	**-**	**0.47**	**0.11**		**0.2**	**0.14**	**Bal.**
Alloy 800H	**19.7**	**31.9**	**0.49**	**-**	**0.51**	**0.94**	**0.07**	**0.50**	**-**	**-**	**Bal.**

3. Microstructural analysis

This section summarizes the results obtained from microstructural investigations of 800H and EUROFER97 alloys.

The grain structure of 800H alloy is shown in Figure 1. The material exhibits relatively large, equiaxed grains decorated with annealing twins. SEM observations revealed that grain interiors and triple junctions are decorated with precipitates of low number density (Figure 2). The precipitate size ranges from ~2 μm to 40 μm. Energy-dispersive X-ray spectroscopy (EDS) identified these precipitates as Ti(C,N).

Transmission electron microscopy (TEM) analysis of helium-implanted EUROFER97 revealed an increased dislocation density (Figure 3). However, no helium bubbles or voids were detected within the investigated depth (up to 6 μm from the surface).

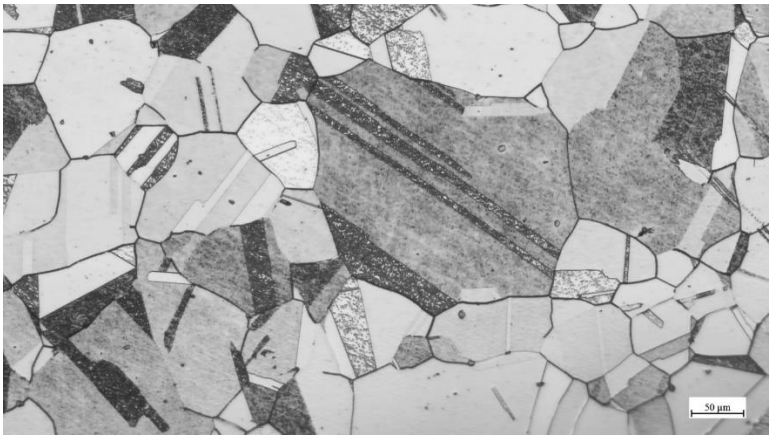


Figure 1. Microstructure of as-received 800H.

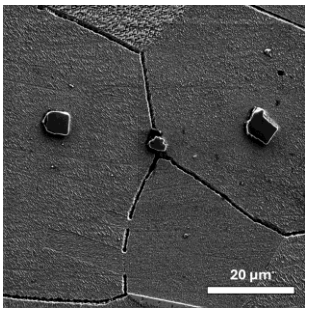


Figure 2. SEM micrograph showing the details of precipitates in 800H.

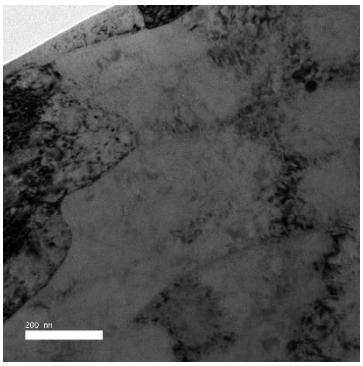


Figure 3. TEM micrograph showing increased dislocation density.

Small-angle neutron scattering (SANS) measurements were carried out on both as-received and irradiated specimens at the D33 instrument at ILL Grenoble. This technique is suitable for analyzing inhomogeneities in the size range of 5–3000 Å. The schematic of the experimental setup is presented in

Figure *4*. Measurements were performed at room temperature in the q-range 0.005–0.5 $Å^{-1}$, using two sample-to-detector distances at a neutron wavelength of 4.5 Å. Additional measurements were taken under a saturation magnetic field (~1.5 T) applied perpendicular to the neutron beam. An example of a SANS spectrum obtained from EUROFER97 is shown in Figure 5.

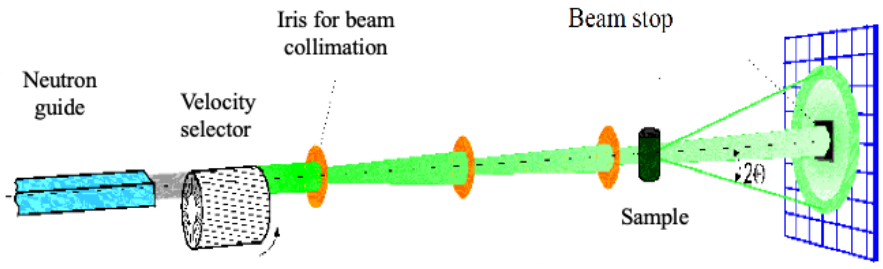


Figure 4. Schematics of SANS setup.

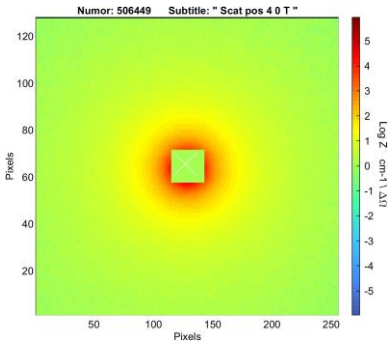


Figure 5. Scattered intensity recorded on the 2D SANS detector.

The evaluated intensity curves are presented in

Figure 6. For helium-implanted EUROFER97, a slight increase in scattering intensity was observed at high *q*-values, indicating the presence of small irradiation-induced inhomogeneities. For comparison, results obtained for ODS EUROFER97 (EUROFER97 strengthened with oxide particles) are shown in

Figure 7. In this case, the intensity curves for as-received and helium-implanted specimens are nearly identical, demonstrating that no measurable irradiation-induced changes occurred within the SANS detection range.

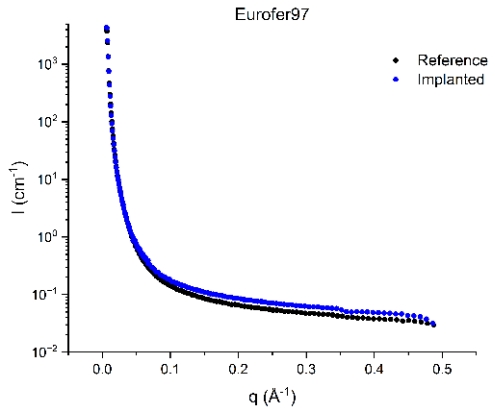


Figure 6. Integrated SANS intensity EUROFER97.

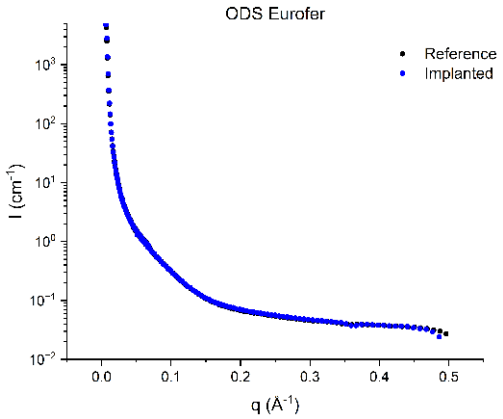


Figure 7. Measured SANS intensity ODS EUROFER97.

The availability of a thick helium-implanted layer also enabled the use of conventional positron annihilation spectroscopy (PAS) with a radioisotope 22Na positron source. This source provides positrons with a continuous energy spectrum up to 540 keV, corresponding to ~85–90% positron stopping within a depth of 65 µm. PAS measurements were performed on a combined lifetime–Doppler spectrometer equipped with three BaF_2 scintillators for lifetime measurements and two HPGe detectors for coincidence Doppler broadening spectroscopy (CDBS) of the annihilation gamma line.

Positron lifetime data obtained from as-received and helium-implanted EUROFER97 and 800H are shown in Figure 8 and Figure 9. Evaluation was based on the established correlation between positron lifetime and vacancy cluster size. The results indicate that alloy 800H exhibits greater resistance to irradiation-induced defect clustering compared to EUROFER97. The estimated bubble size from PAS measurements is below 0.5 nm, which is consistent with both SANS and TEM observations.

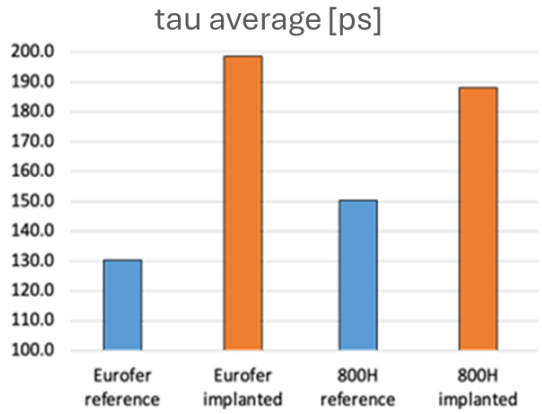


Figure 8. Measured PAS mean life times.

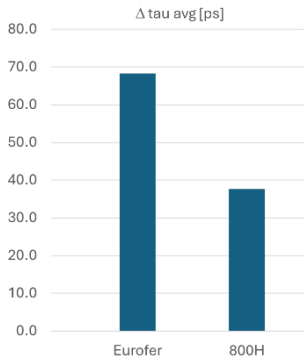


Figure 9. Change in PAS mean lifetimes.

4. Nanoindentation testing

4.1. Experiments

The nanoindentation testing was performed using the Hysitron TI Premier nano indenter (

Figure 10) equipped with a Berkovich diamond tip. The tip area function and the instrument stiffness were calibrated using fused silica reference material with known elastic modulus.

Two types of loading methods were used: the standard trapezoidal following a pattern of 5s loading, 2s hold and 5s unloading and cyclic method, when the load is gradually increased at a single location through multiple loading and unloading cycles. The cyclic method allows to obtain the indentation hardness as a function of depth from a single indent. For both methods a maximum force of 13 mN was used. The complete load cycles are shown in Figure *11*.



Figure 10. Hysitron TI Premier Nanoindenter

49 measurements were taken with each method, arranged into 7x7 grid, with distance of 15 µm between the neighboring points. Data analysis was done by means of the Oliver-Pharr method [1], [2].

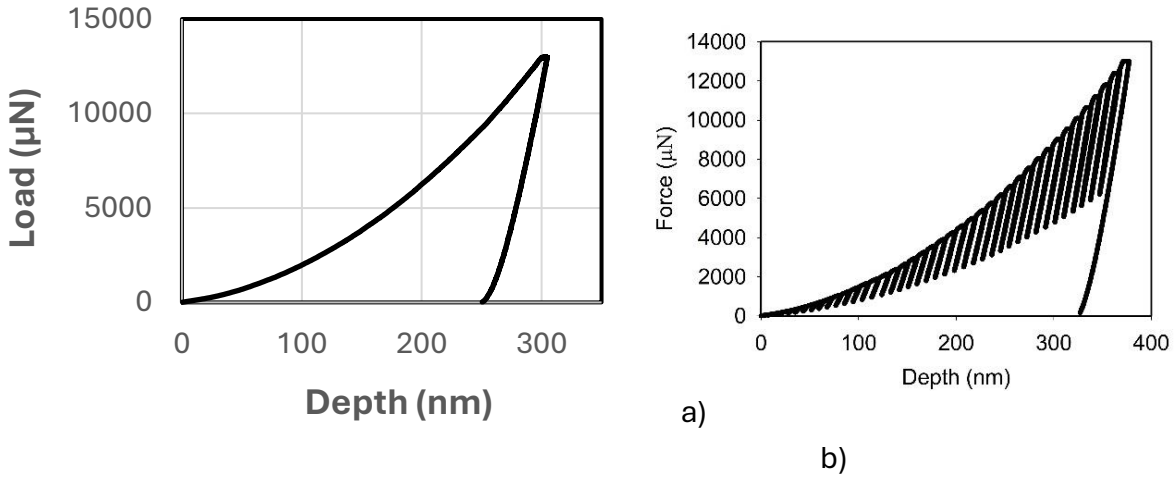


Figure 11. Typical Indentation curves for a) trapezoid method, b) cyclic method.

This method is using the unloading curve to determine the contact stiffness, S, which is defined as the slope of the unloading curve at maximum displacement:

$$S = dP/dh \qquad (1)$$

where P is the applied load and h is the indentation depth. The contact stiffness is then used to calculate the reduced elastic modulus E_r:

$$E_r = \frac{S}{2\sqrt{\pi A}} \qquad (2)$$

where A is the projected contact area at the maximum depth, typically determined using a pre-calibrated area function dependent on the geometry of the indenter (e.g., a Berkovich indenter). The elastic modulus of the material E is obtained from the reduced modulus by accounting for the elastic properties of the indenter:

$$\frac{1}{E_r} = \frac{1-v^2}{E} + \frac{1-v_i^2}{E_i} \qquad (3)$$

where v and v_i are the Poisson's ratios of the material and indenter, respectively, and E_i is the elastic modulus of the indenter.

The hardness H is calculated as the applied maximum load $P_{\max}$ divided by the projected contact area A:

$$H = \frac{P_{\max}}{A} \qquad (4)$$

4.2. Results

The averaged load-displacement indentation curves from 49 measurements are presented in Figure 12 for EUROFER97 steel in both as-received and ion-irradiated conditions. There is a clear decrease in maximum indentation depth and in the slope of the loading curve is observed after irradiation, indicating irradiation-induced hardening. From the individual loading curves, the indentation modulus, contact depth and hardness were extracted. The average values are summarized in Figure 13.

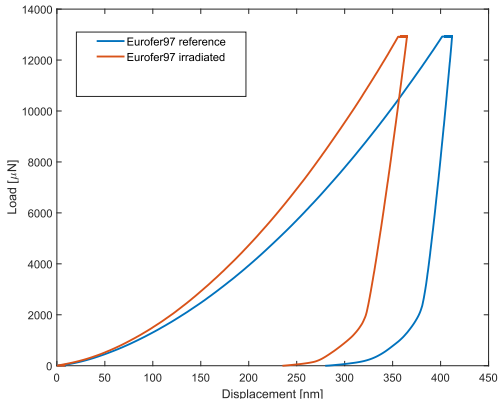


Figure 12. Averege Load vs. Displacement curves on EUROFER97.

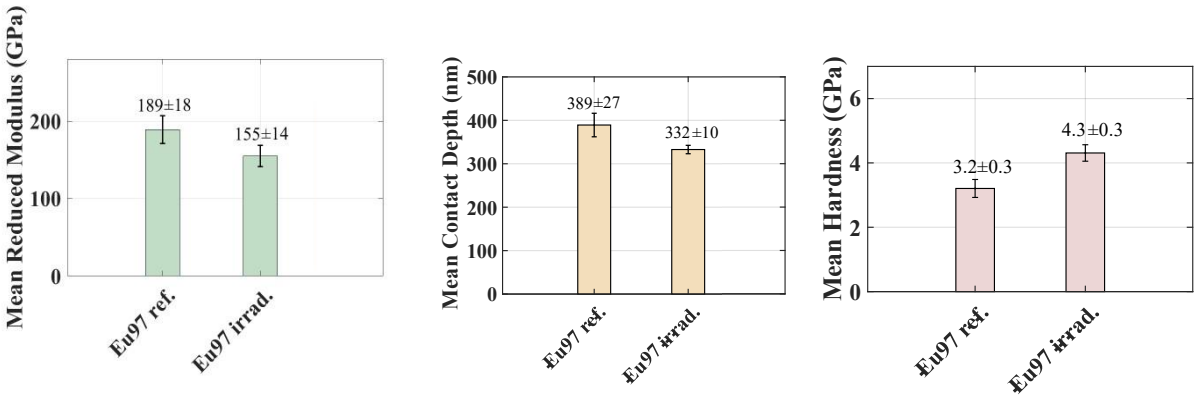


Figure 13. The mean characteristic values evaluated from nanoindentation measurement of EUROFER97.

For EUROFER97 , ion-irradiation led to a hardness increase of 1.1 GPa compared with the unirradiated condition, confirming significant irradiation-induced hardening. At the same time, a reduction of ~17% in the reduced modulus was observed. The cause of this decrease remains unclear and needs further investigation.

The results from single indentation for 800H alloy are shown in Figures 5 and 6, with a representative 5 × 5 indentation array presented in Figure 7. In this case, both hardness and indentation modulus increased after irradiation, again consistent with radiation-induced hardening. However, the magnitude of hardening in 800H was less pronounced than in EUROFER97. A direct comparison (Figure 8) shows that the relative increase in hardness for 800H is approximately half that observed in EUROFER97. For reference, the relative hardening of ODS-reinforced EUROFER97 is also included in Figure 8, illustrating the strengthening effect of nanoscale oxide particles.

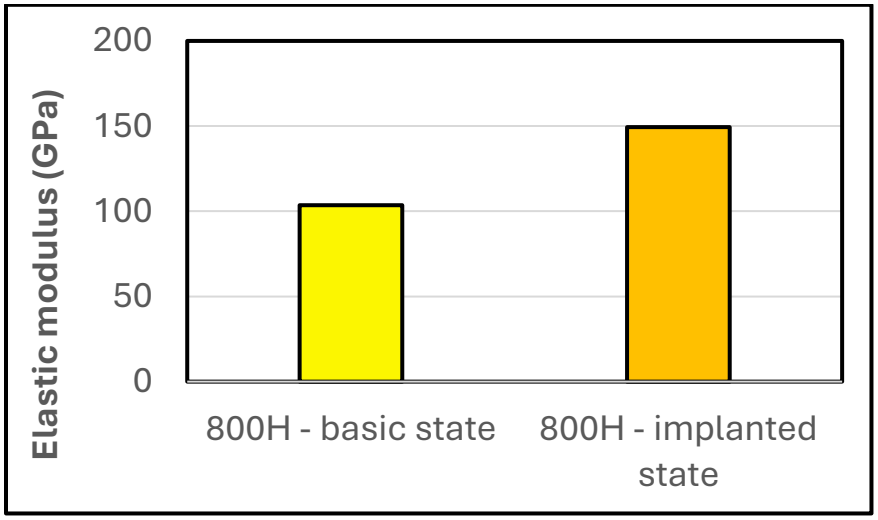


Figure 14. Elastic modulus of 800H, as-received vs implanted state.

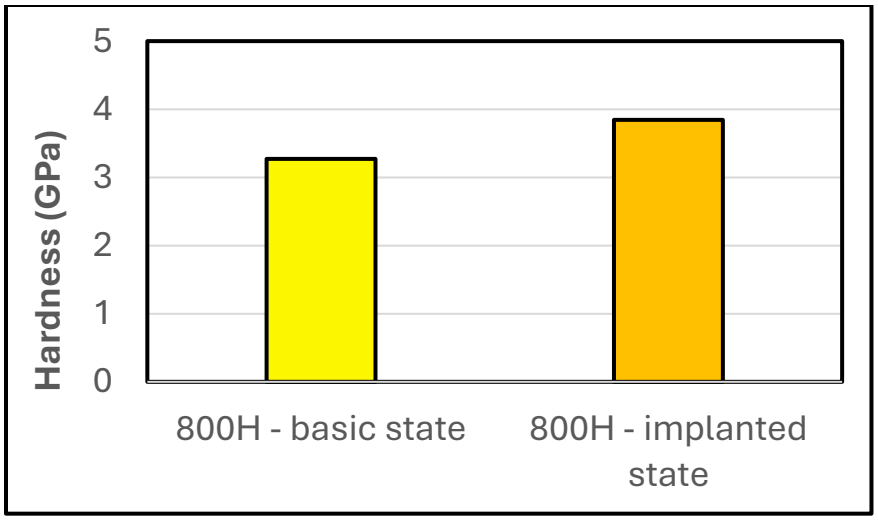


Figure 15. Hardness of 800H in as-received and implanted state.

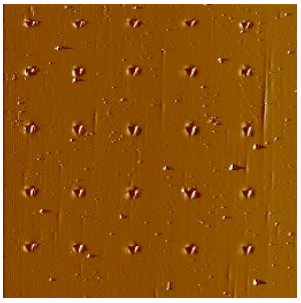


Figure 16. Indents in He irradiated 800H, 80x80μm^2.

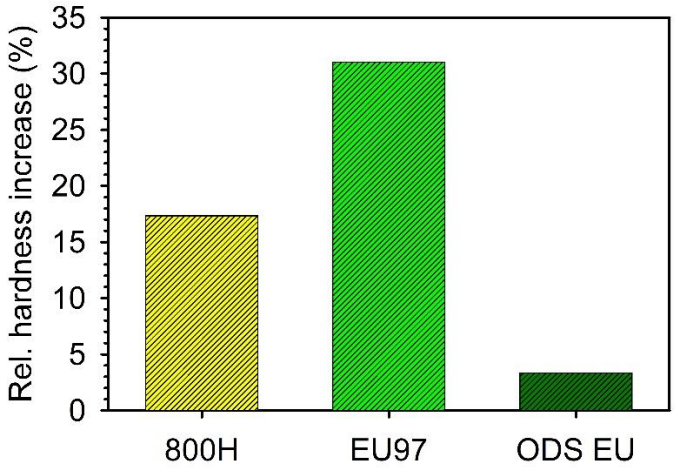


Figure 17. Relative increase of hardness after helium implantation.

Results obtained from the cyclic nanoindentation method are shown in *Figure 18*. Each curve represents an average of 49 cyclic measurements. Across the entire measured depth range, the irradiated material exhibited higher hardness compared with the unirradiated state, confirming consistent irradiation-induced hardening. In unirradiated material, indentation hardness increased with decreasing contact depth, asymptotically approaching the single-indentation hardness value at large depths. This behavior reflects the well-known indentation size effect (ISE), which can arise from experimental or surface preparation artefacts but may also be an intrinsic property of the material [3,4].

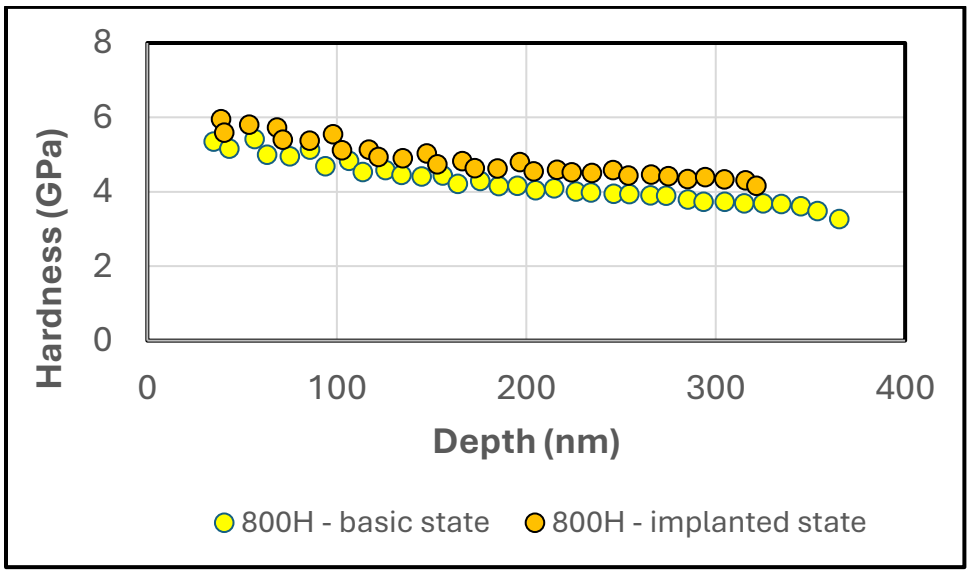


Figure 18. Hardness as a function of penetration depth for 800H in as-received and irradiated states.

5. Summary

This report has presented the results of microstructural and micromechanical investigations performed on ion-irradiated specimens of EUROFER97 and alloy 800H, two key candidate materials for advanced nuclear systems.

Microstructural characterization provided complementary insights. SEM and TEM investigations identified precipitates and increased dislocation density in the irradiated materials but did not reveal visible helium bubbles or voids within the analyzed depth range. SANS measurements detected subtle irradiation-induced inhomogeneities in EUROFER97, whereas ODS-reinforced EUROFER97 showed no measurable change, highlighting the beneficial effect of oxide dispersion strengthening. PAS experiments, enabled by the thick helium-implanted layers, confirmed the presence of vacancy-type defects and indicated that helium bubble sizes remained below 0.5 nm, consistent with SANS and TEM results.

Nanoindentation measurements demonstrated irradiation-induced hardening in both materials. EUROFER97 exhibited a hardness increase of ~1.1 GPa, accompanied by a reduction of ~17% in reduced modulus, suggesting a more pronounced change in mechanical properties. In contrast, alloy 800H showed a smaller relative increase in hardness, approximately half of that observed in EUROFER97, indicating comparatively higher resistance to irradiation-induced hardening. The indentation size effect (ISE) was consistently observed in unirradiated specimens and confirmed through cyclic indentation testing.

In conclusion, the combined microstructural and nanoindentation results establish a clear link between irradiation conditions, defect evolution, and mechanical property changes. The findings underline the importance of alloy composition and microstructural reinforcement in mitigating helium-induced damage. These results provide a solid basis for further investigations within ARTHEMIS, particularly in relation to micromechanical testing and studies of synergistic effects involving irradiation and environmental exposure.

6. References

[1] W. C. Oliver, G. M. Pharr, *J. Mater. Res.*, 7 (1992) 1564–1583.

[2] W. C. Oliver, G. M. Pharr, *J. Mater. Res.*, 19 (2004) 3–20.

[3] W. D. Nix, H. Gao, *J. Mech. Phys. Solids*, 46 (1998) 411–425.

[4] G. M. Pharr, E. G. Herbert, Y. Gao, *Annu. Rev. Mater. Res.*, 40 (2010) 271–292.